
PAPER: CLASSICAL STATISTICAL MECHANICS, EQUILIBRIUM AND NON-EQUILIBRIUM

The study of percolation with the presence of extended impurities

To cite this article: I Lonarevi *et al* *J. Stat. Mech.* (2017) 093202

View the [article online](#) for updates and enhancements.

The study of percolation with the presence of extended impurities

I Lončarević¹, Lj Budinski-Petković¹, D Dujak², A Karač³,
Z M Jakšić⁴ and S B Vrhovac^{4,5}

¹ Faculty of Technical Sciences, University of Novi Sad, Trg D. Obradovića 6, Novi Sad 21000, Serbia

² Faculty of Metallurgy and Materials, University of Zenica, Bosnia and Herzegovina

³ Polytechnic faculty, University of Zenica, Bosnia and Herzegovina

⁴ Scientific Computing Laboratory, Center for the Study of Complex Systems, Institute of Physics Belgrade, University of Belgrade, Pregrevice 118, Zemun 11080, Belgrade, Serbia

E-mail: vrhovac@ipb.ac.rs

Received 10 May 2017

Accepted for publication 19 July 2017

Published 18 September 2017



CrossMark

Online at stacks.iop.org/JSTAT/2017/093202
<https://doi.org/10.1088/1742-5468/aa82c0>

Abstract. In the preceding paper, Budinski-Petković *et al* (2016 *J. Stat. Mech.* 053101) studied jamming and percolation aspects of random sequential adsorption of extended shapes onto a triangular lattice initially covered with point-like impurities at various concentrations. Here we extend this analysis to needle-like impurities of various lengths ℓ . For a wide range of impurity concentrations p , percolation threshold θ_p^* is determined for k -mers, angled objects and triangles of two different sizes. For sufficiently large impurities, percolation threshold θ_p^* of all examined objects increases with concentration p , and this increase is more prominent for impurities of a larger length ℓ . We determine the critical concentrations of defects p_c^* above which it is not possible to achieve percolation for a given object, for impurities of various lengths ℓ . It is found that the critical concentration p_c^* of finite-size impurities decreases with the length ℓ of impurities. In the case of deposition of larger objects an exception occurs for point-like impurities when critical concentration p_c^* of monomers is lower than p_c^* for the dimer impurities. At relatively low concentrations p , the presence of small impurities (but not point-like) stimulates the percolation for larger depositing objects.

⁵ www.ipb.ac.rs/~vrhovac/

Keywords: classical Monte Carlo simulations, percolation problems, defects, adsorbates and surfactants

Contents

1. Introduction	2
2. Definition of the model and the simulation method	5
3. Results and discussion	6
4. Summary	18
Acknowledgments	18
References	19

1. Introduction

Understanding the various aspects of effective attachment of particles to surfaces, involving transport, adsorption and adhesion steps, is important for many practical processes such as water filtration, electroflotation, separation of toner and ink particles, coating formation, paper making, xerography, catalysis, colloid lithography, protein and cell separation, food emulsion and foam stabilization, immobilization of enzymes, immunological assays, etc [1]. Depositing objects range in size from the micrometer scale down to nanometer scale, and depending on the application in question, the objects could be colloidal particles, polymer chains, globular proteins, nanotubes, DNA segments, etc. Deposition processes in which deposited particles can neither diffuse along, nor desorb from the substrate on the time scales of the dense coverage formation can be studied as random sequential adsorption (RSA).

In the simplest RSA model particles are randomly, sequentially and irreversibly deposited onto a substrate without overlapping each other. The kinetic properties of a deposition process are described by the time evolution of the coverage $\theta(t)$, which is the fraction of lattice sites covered at time t by the deposited particles. Within a monolayer deposit, each adsorbed particle affects the geometry of all later placements. Due to the blocking of the substrate area by the previously adsorbed particles, at large times the coverage approaches the jammed-state value θ_J , where only gaps too small to accommodate new particles are left in the monolayer. For a comprehensive review of RSA models see, e.g. [2–5].

During the process of irreversible deposition the number of deposited objects increases causing the growth of clusters of nearest-neighbor occupied sites. Percolation assumes the existence of a large cluster that reaches two opposite sides of the substrate [6]. Formation of a long-range connectivity in disordered systems attracts a considerable interest [7–17, 18] thanks to its applications in numerous practical problems such

as conductivity in composite materials, flow through porous media, polymerization, gelation, behavior of scale-free random networks such as the Internet [19], and even some phenomena in sociological systems [20].

In many studies of RSA the main attention is focused on deposition of regular shapes on spatially homogeneous, regular substrates [2], but recent interest has shifted to deposition of irregular objects on pre-patterned or otherwise structured or inhomogeneous surfaces [5, 21–24]. In real experimental situations these include minerals, pigments, biological membranes, wafers and other substrates that are inherently heterogeneous. When the scale of surface inhomogeneities is comparable to the object size, the underlying pattern alters the surface-particle interaction, thus imposing modified morphology and dynamics of the deposition process. It is of theoretical and experimental interest to understand and analyze how specific surface modifications affect the structure of deposited layers, late-stage kinetics and percolation properties of the deposition process, etc.

In modeling real deposition processes, one often needs to take into account the possibility of contaminations or defects that interfere the deposition of primary particles and introduce a disorder into the system. Many important findings regarding the jamming and percolation of various objects on disordered (or heterogeneous) substrates with defects (or impurities) have been reported over the past two decades. The impact of defects on the jamming and percolation in RSA of k -mers on a square lattice is studied in [25–30]. Cornette *et al* [25, 26] investigated numerically both the bond and the site percolation problems for self-avoiding walk k -mers in the presence of impurities. The contaminated lattice is built by randomly selecting a fraction of the elements of the lattice (either bonds or sites) that are considered forbidden for deposition. This research suggests that the concentration of impurities at which percolation becomes impossible decreases rapidly with increasing values of k . By the same model, Cornette *et al* [27] have analyzed the kinetics of the RSA process.

Centres and Ramirez-Pastor [28] have investigated the dependence of percolation and jamming thresholds of linear k -mers on the concentration of defects for different values of k , ranging from 2 to 64. They reported that for each fixed value of k , percolation can occur when fraction of imperfect bonds ρ is smaller than critical concentration of defects ρ_k^* at which percolation is possible only at jamming coverage. It was also shown that in the range $0 \leq \rho \leq \rho_k^*$, the percolation threshold is practically independent on the fraction of defects.

In [29], two models are analyzed—in the first one it is assumed that some fraction of sites is initially occupied by nonconducting point defects, and in the second one that some fraction of the sites in the k -mers is nonconducting. The dependence of the percolation threshold on the length of the k -mers and on the impurity concentration is analyzed. Above some critical concentration of defects, percolation is blocked even at the jamming limit. The authors have found that percolation of k -mers is impossible even for an ideal lattice if the size k exceeds a certain critical value. Recently, Tarashevich *et al* [30] have studied the influence of defects on the behaviour of electrical conductivity in a monolayer produced by the isotropic and anisotropic deposition of k -mers onto a square lattice. Two kinds of defects are involved into consideration. The defects in the substrate (impurities) prevent deposition of the particles. Additionally, it is supposed that some parts of the k -mers may be either conducting or non-conducting (defective).

Calculation of the electrical conductivities gave an explicit confirmation that even a very small concentration of any kinds of defects has strong impact on the electrical conductivity.

Kondrat [31, 32] extended the study of the influence of defects on jamming and percolation aspect of irreversible deposition to the triangular lattice and stick-shaped impurities. However, process of percolation cluster formation has been considered for point-like conductors only. The results obtained revealed that: for sufficiently low level of finite-size impurities the percolation threshold increases with the impurity concentration; this effect is more apparent for larger size impurities; there exists a characteristic value of impurity concentration (that depends on the size of impurity particles) above which the percolation threshold in the system becomes a decreasing function.

The analysis of more complex case of extended particles of both kinds (conductors and insulators) is a subject of present paper. Here we present the results of extensive simulations of irreversible deposition of objects of various shapes on a planar triangular lattice initially covered with needle-like impurities at various concentrations. The depositing objects are made by directed self-avoiding steps on the triangular lattice. Jamming coverages θ_J and the percolation thresholds θ_p^* are determined for a wide range of impurity concentrations p . Our present work is a continuation of the recently published article [33] which described the percolation and jamming properties of the same system, but only in the presence of point-like impurities. It has been shown that, for k -mers and angled objects, the percolation threshold monotonically decreases with the size of the objects. However, in the case of more regular and compact shapes (triangles), the percolation threshold monotonically increases with the object size. In both cases, the percolation threshold is found to be practically insensitive to the point-like defect concentration. We have pointed out that percolation can be reached at highest concentrations of impurities with angled objects. Triangles have the lowest values of critical concentrations and the worst performance regarding percolation.

It should be emphasized that the degree of disorder of the surface is tunable in our model not only by selecting the value of the impurity concentration, but also with the choice of the shape or size of impurities. The growing interest in such surface properties stems from their practical significance as thin films filled with the hybrid and functionalized single- and multi-walled carbon nanotubes [34]. Modifications of tubular structures usually include the presence of inorganic or organic functional groups, direct incorporation of specific elements, and generation of insulating defects [35]. Consequently, influence both of the point-like insulating defects and the finite-size impurities on the electrical connectivity of monolayer needs an additional attention. In this work we want to analyze how the length of needle-like impurity particles interferes the percolation process of extended primary particles (k -mers, angled objects and triangles). For each given impurity, we determine a critical concentration of defects p_c^* above which it is not possible to achieve the percolation. We provide a detailed description of two different methods for calculation of the critical concentrations p_c^* for arbitrary impurity. Critical concentrations are obtained using the finite-size scaling analysis of the probability $P(p; L)$ that the percolation cluster of deposited objects is not formed during the simulation run on a lattice of size L , initially covered with impurities at various concentrations p . In addition, the values of critical concentration p_c^* can be

Table 1. The jamming coverages θ_J and the percolation thresholds θ_p^* for line segments (A_1) , (A_2) , (A_3) , (A_4) , (A_5) , and (A_7) of different lengths $\ell^{(x)}$. The numbers in parentheses are the numerical values of the standard uncertainty of $\theta_J^{(x)}$ and θ_p^* referred to the last digits of the quoted value.

Impurities	(x)	$\ell^{(x)}$	θ_J	θ_p^*
•	(A_0)	0	1	0.5000(1)
••	(A_1)	1	0.914033(3)	0.4867(1)
•••	(A_2)	2	0.836211(4)	0.4628(3)
••••	(A_3)	3	0.789090(6)	0.4432(2)
•••••	(A_4)	4	0.758458(7)	0.4299(4)
••••••	(A_5)	5	0.737031(9)	0.4206(5)
•••••••	(A_7)	7	0.708962(12)	0.4124(6)

obtained in the intersection point of the dependences of the jamming density $\theta_J(p)$ and the percolation threshold $\theta_p^*(p)$ on the concentration of impurities p .

The paper is organized as follows. Section 2 describes the details of the model and the simulations. We give the simulation results and discussions in section 3. Finally, section 4 contains some additional comments and final remarks.

2. Definition of the model and the simulation method

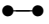
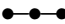




In our model the substrate is a triangular lattice initially occupied by defects (impurities) of various sizes at effective concentration p . This concentration is defined as a fraction of sites of the lattice that are occupied by defects. Impurities (I) are k -mers of length $\ell = 0-5, 7$, shown in table 1 as objects (A_0) – (A_5) , and (A_7) . Particles of impurity cannot overlap and their spatial distribution at density p is generated using the RSA method. In this way we are able to prepare the substrate in disordered initial state with a statistically reproducible density p of impurities.

Depositing objects (O) are made by directed self-avoiding steps of length ℓ . Special attention has been paid to deposition of shapes shown in table 2: k -mers, angled objects and triangles of two different sizes. Objects of a larger size are made by repeating each step of a basic shape the same number of times. Exception is made for triangles, where larger objects also occupy all comprised sites.

After placing impurities (I) up to a chosen concentration p , we switch the impurity deposition events off and initiate the second step of the experiment—adsorption of the objects (O) (‘conductors’). At each Monte Carlo step a lattice site is selected at random. If the selected site is unoccupied, deposition of the object is tried in one of the six orientations. We fix the beginning of the walk that makes the shape at the selected site and search whether all successive ℓ sites are unoccupied. If so, we occupy these $\ell + 1$ sites and place the object. If the attempt fails, a new site and a new direction are selected at random.

The Monte Carlo simulations are performed on a triangular lattice of a size up to $L = 3200$. Periodic boundary conditions are used in all directions. The time is counted by the number of attempts to select a lattice site and scaled by the total number of

Table 2. The jamming coverages θ_J and the percolation thresholds θ_p^* for line segments (A_1), (A_2), angled objects (B_2), (B_4), and triangles (C_2), (C_5) of different lengths $\ell^{(x)}$. The numbers in parentheses are the numerical values of the standard uncertainty of $\theta_J^{(x)}$ and θ_p^* referred to the last digits of the quoted value.

Objects	(x)	$\ell^{(x)}$	$n_s^{(x)}$	θ_J	θ_p^*
	(A_1)	1	2	0.914 033(3)	0.4867(1)
	(A_2)	2	2	0.836 211(4)	0.4628(3)
	(B_2)	2	1	0.834 440(4)	0.4606(6)
	(B_4)	4	1	0.717 995(7)	0.4147(4)
	(C_2)	2	3	0.796 940(5)	0.5246(1)
	(C_5)	5	3	0.721 062(7)	0.5529(6)

lattice sites. The data are averaged over 500 or 5000 independent runs for each of the investigated ((O) , (I)) pairs, and for each density p of impurities (I).

The jamming limit θ_J is reached when no more objects can be placed in any position on the lattice. In practice, during the simulation we record the number of all inaccessible sites in the lattice. These include the occupied sites and the sites that are unoccupied but cannot be the beginning of the walk deposited in any of the six orientations. The jamming limit is reached when the number of inaccessible sites is equal to the total number of sites in the lattice. Checking this condition is performed after every L^2 attempts (unit time) to absorb the object. If the condition is false, we stop the current run and continue with the next simulation run.

Impact of the impurity length ℓ on percolation is studied. The coverage of the surface is increased in the RSA process up to the percolation threshold θ_p , when there appears a cluster that extends through the whole system along one of the three directions of the lattice. The tree-based union/find algorithm was used to determine the percolation threshold [36, 37]. Each cluster of connected sites is stored as a separate tree, having a single ‘root’ site. All sites of the cluster possess pointers to the root site, so it is simple to ascertain whether two sites are members of the same cluster. When a deposited object connects two separate clusters, they are amalgamated by adding a pointer from the root of the smaller cluster to the root of the larger one. This procedure is repeated until the percolation threshold is reached, i.e. until the opposite sides of the lattice are connected by a simple cluster.

3. Results and discussion

Values of the percolation thresholds for the infinitely large lattice θ_p^* are obtained using the usual finite-size scaling analysis of the percolation behavior on two-dimensional lattices [6]. In such systems one assumes that the effective percolation threshold θ_p (the mean value of threshold measured for a finite lattice) approaches the asymptotic value $\theta_p \rightarrow \theta_p^*$ ($L \rightarrow \infty$) via the power law:

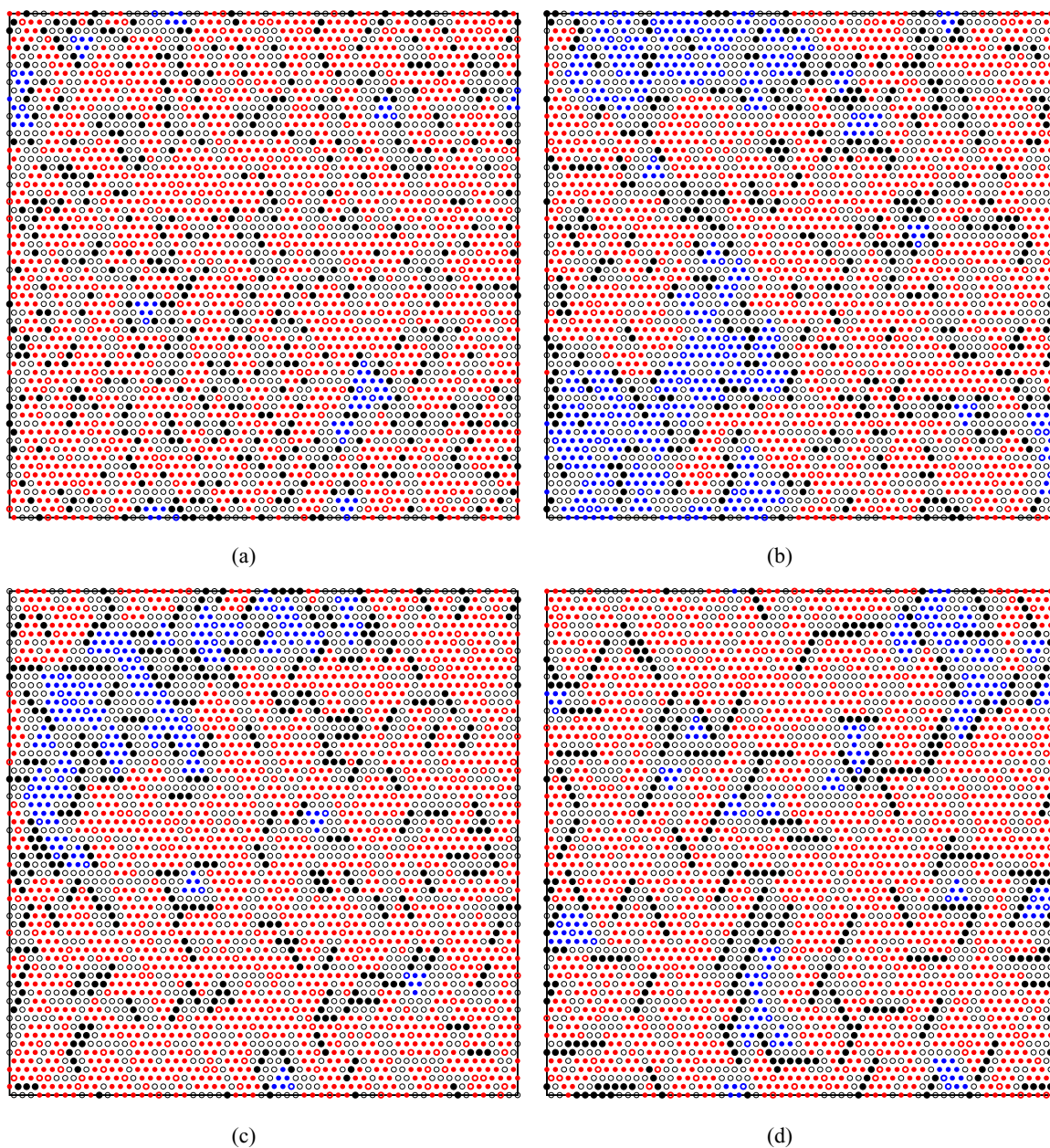


Figure 1. Typical configurations of deposited object (C_5) (see table 2) at the percolation threshold obtained for impurities: (a) (A_0), (b) (A_1), (c) (A_2), and (d) (A_4) from table 1. The snapshots are given for impurity concentration $p = 0.12$. The corresponding values of the percolation threshold θ_p , measured for a finite lattice of size $L = 60$, are indicated below the figures. Deposited objects that belong to the percolation cluster are colored in red. Deposited objects outside of the percolation cluster are colored in blue. Impurities and empty nodes are black and white, respectively. Opened circles represent the head of the objects (the beginning of the walk). (a) (C_5) + (A_0), $\theta_p = 0.5483$. (b) (C_5) + (A_1), $\theta_p = 0.5433$. (c) (C_5) + (A_2), $\theta_p = 0.5517$. (d) (C_5) + (A_4), $\theta_p = 0.5617$.

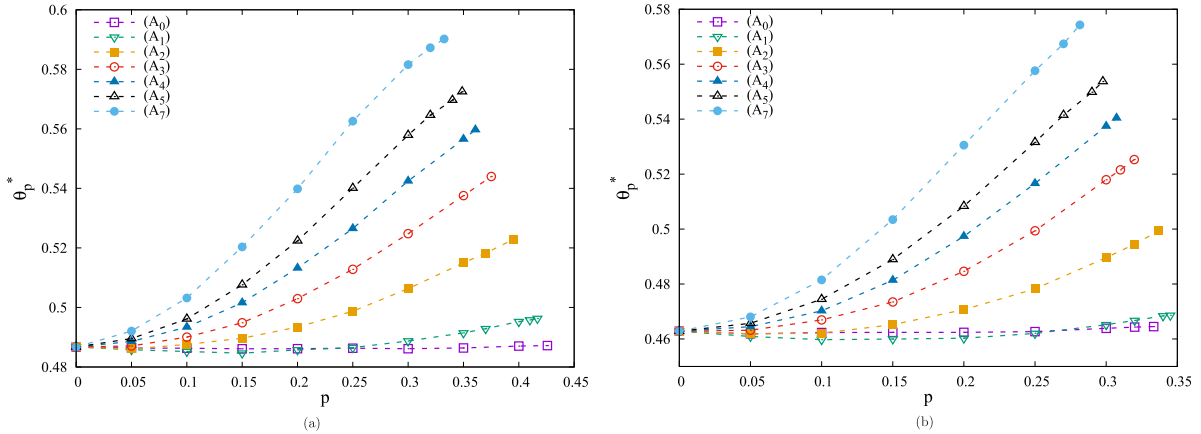


Figure 2. Percolation thresholds θ_p^* versus the impurity concentration p for line segments (a) (A_1) , and (b) (A_2) from table 2. The results are given for various impurities, as indicated in the legend (see table 1).

$$\theta_p - \theta_p^* \propto L^{-1/\nu}. \tag{1}$$

Here the constant ν is the critical exponent that governs the divergence of the correlation length as $\xi \propto |\theta_p - \theta_p^*|^{-\nu}$. It should be noticed that the universality class of random percolation in two dimensions is very well identified and the critical exponents are known exactly, namely, $\nu = 4/3$ [6]. In our study, the typical values of lattice size are $L = 40, 60, 80, 100, 200, 400, 800, 1600, 3200$.

In figure 1 we show the typical snapshot configurations at the percolation threshold obtained for object (C_5) (see table 2) and impurities (a) (A_0) , (b) (A_1) , (c) (A_2) , and (d) (A_4) from table 1. The snapshots are taken at the impurity concentration $p = 0.12$. Different colors correspond to clusters of connected sites and the percolating clusters are clearly observed. The mesh structure of the open spaces look very different for adsorbing point-like impurities (A_0) in comparison with the extended impurities. Deposition of elongated impurities is characterized by domains of large islands of unoccupied sites (see, e.g. figure 1(d)). On the other hand, small impurities such as monomers (A_0) cover the surface more uniformly (see figure 1(a)), so that empty space on the lattice is broken into small areas.

Dependence of the percolation threshold θ_p^* on the impurity concentration p is shown in figures 2–4 for various lengths ℓ of impurities and for depositing objects shown in table 2. The last given point in all these graphs corresponds to the critical defect concentration p_c^* at which the percolation can be obtained. More precisely, concentration of the impurities p is below/above the critical density p_c^* , if the probability of the formation of percolation cluster tends to unity/zero as the lattice size increases, $L \rightarrow \infty$. The ordinate of the last point is equal to the limiting threshold $\theta_p^c = \lim_{p \rightarrow p_c^*} \theta_p^*(p)$, which we call the ‘critical percolation threshold’. Detailed description of the methods for calculation of critical densities p_c^* and thresholds θ_p^c are provided later in the text. Results in figure 2(a), obtained for deposition of dimers (A_1) , suggest that the percolation threshold θ_p^* is practically not affected by the presence of point-like impurities (A_0) . However, when increasing the length ℓ of impurities, percolation threshold θ_p^* increases with p . The critical defect concentration p_c^* decreases with the length ℓ of

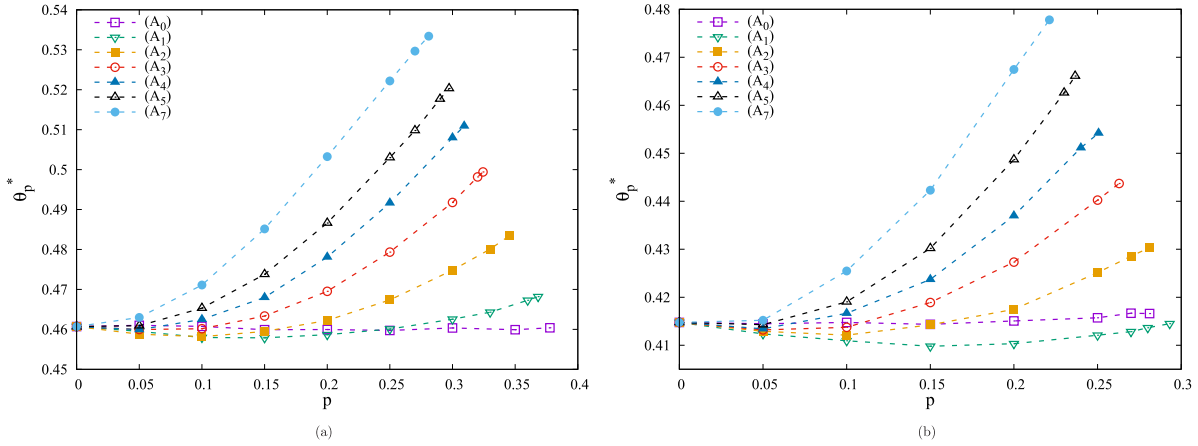


Figure 3. Percolation thresholds θ_p^* versus the impurity concentration p for angled objects: (a) (B_2), and (b) (B_4) from table 2. The results are given for various impurities, as indicated in the legend (see table 1).

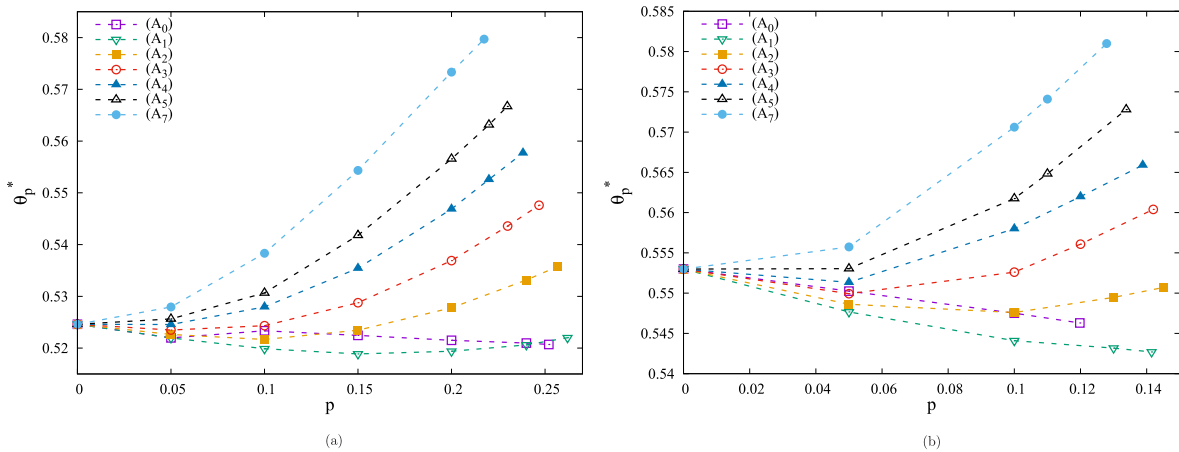


Figure 4. Percolation thresholds θ_p^* versus the impurity concentration p for triangles: (a) (C_2), and (b) (C_5) from table 2. The results are given for various impurities, as indicated in the legend (see table 1).

the impurities. When deposited objects are line segments (A_2) covering three sites (see figure 2(b)), the critical defect concentrations p_c^* are lower, and we can see a slight difference concerning the p_c^* in the case of point-like impurities (A_0) and dimer impurities (A_1); critical concentration p_c^* for the point-like impurities (A_0) is now a little bit lower than for the dimer impurities (A_1).

In figure 3(a) results for the percolation thresholds θ_p^* versus the concentration p of impurities of different lengths ℓ are shown for the depositing object (B_2)—the angled object made of two steps. These results are qualitatively similar to those for the deposition of dimers (A_1), but the percolation thresholds θ_p^* , and also the critical concentrations p_c^* , are lower. Results for the angled object (B_4), made of four steps, are shown in figure 3(b). As in figure 2(b), here the critical concentration p_c^* is slightly lower for the point-like impurities (A_0) than for the dimer impurities (A_1). Also, the percolation thresholds θ_p^* are noticeably lower for the dimer (A_1) than for the point-like impurities (A_0) in the whole range of impurity concentrations.

Table 3. Shown here is the number of independent simulation runs (out of 500) during which the percolation cluster is not formed, for densities $p =$ (a) 0.1, (b) 0.2, (c) 0.3, (d) 0.4 of impurity (A_4) and for lattices of size $L = 40 - 3200$. The cases without percolation clusters in 500 simulation runs are in bold, while the cases where percolation cluster is formed in each run are in italic. The results are shown for all objects from table 2.

(a) $p = 0.1$						
L	(A_1)	(A_2)	(B_2)	(B_4)	(C_2)	(C_5)
40	<i>0</i>	<i>0</i>	<i>0</i>	<i>0</i>	<i>0</i>	14
60	<i>0</i>	<i>0</i>	<i>0</i>	<i>0</i>	<i>0</i>	6
80	<i>0</i>	<i>0</i>	<i>0</i>	<i>0</i>	<i>0</i>	1
100	<i>0</i>	<i>0</i>	<i>0</i>	<i>0</i>	<i>0</i>	2
200	<i>0</i>	<i>0</i>	<i>0</i>	<i>0</i>	<i>0</i>	<i>0</i>
400	<i>0</i>	<i>0</i>	<i>0</i>	<i>0</i>	<i>0</i>	<i>0</i>
800	<i>0</i>	<i>0</i>	<i>0</i>	<i>0</i>	<i>0</i>	<i>0</i>
1600	<i>0</i>	<i>0</i>	<i>0</i>	<i>0</i>	<i>0</i>	<i>0</i>
3200	<i>0</i>	<i>0</i>	<i>0</i>	<i>0</i>	<i>0</i>	<i>0</i>
(b) $p = 0.2$						
L	(A_1)	(A_2)	(B_2)	(B_4)	(C_2)	(C_5)
40	<i>0</i>	<i>0</i>	<i>0</i>	16	17	456
60	<i>0</i>	<i>0</i>	<i>0</i>	1	5	491
80	<i>0</i>	<i>0</i>	<i>0</i>	1	5	490
100	<i>0</i>	<i>0</i>	<i>0</i>	<i>0</i>	1	499
200	<i>0</i>	<i>0</i>	<i>0</i>	<i>0</i>	<i>0</i>	500
400	<i>0</i>	<i>0</i>	<i>0</i>	<i>0</i>	<i>0</i>	500
800	<i>0</i>	<i>0</i>	<i>0</i>	<i>0</i>	<i>0</i>	500
1600	<i>0</i>	<i>0</i>	<i>0</i>	<i>0</i>	<i>0</i>	500
3200	<i>0</i>	<i>0</i>	<i>0</i>	<i>0</i>	<i>0</i>	500
(c) $p = 0.3$						
L	(A_1)	(A_2)	(B_2)	(B_4)	(C_2)	(C_5)
40	5	127	93	414	449	500
60	3	102	86	449	483	500
80	<i>0</i>	84	57	478	497	500
100	<i>0</i>	82	64	489	498	500
200	<i>0</i>	52	33	500	500	500
400	<i>0</i>	27	6	500	500	500
800	<i>0</i>	3	1	500	500	500
1600	<i>0</i>	<i>0</i>	<i>0</i>	500	500	500
3200	<i>0</i>	<i>0</i>	<i>0</i>	500	500	500
(d) $p = 0.4$						
L	(A_1)	(A_2)	(B_2)	(B_4)	(C_2)	(C_5)
40	369	488	496	500	500	500
60	411	498	498	500	500	500
80	461	500	500	500	500	500
100	478	500	500	500	500	500
200	497	500	500	500	500	500
400	500	500	500	500	500	500
800	500	500	500	500	500	500
1600	500	500	500	500	500	500
3200	500	500	500	500	500	500

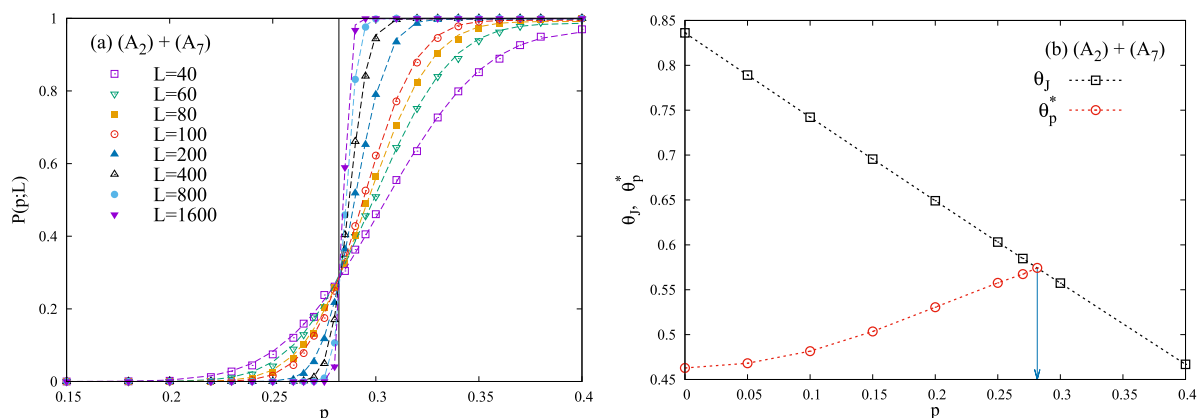


Figure 5. Two methods for determining the critical density p_c : (a) Shown here are the values of the probability $P(p; L)$ that the percolation cluster of deposited objects (A_2) (table 2) is not formed during the simulation run on the lattice of size L (see legend), initially covered with impurities (A_7) (table 1) at various densities p . The dashed superimposed lines are the fits according to equation (2). The thin vertical line indicates the value of fitting parameter $\mu = 0.2821 \pm 0.0010$. (b) Dependences of the jamming density θ_J and the percolation threshold θ_p^* for object (A_2) on the density p of impurity (A_7). The thin vertical arrow indicates the value of critical density $p_c^* = 0.2815$.

Percolation thresholds θ_p^* for deposition of triangles (C_2) and (C_5) are shown in figures 4(a) and (b), respectively. In figure 4(a) the percolation threshold θ_p^* in the case of dimer impurities (A_1) is lower than in the case of point-like impurities (A_0), and this effect is more pronounced for larger triangles (see figure 4(b)). The critical impurity concentration p_c^* for the point-like impurities (A_0) is lower than for the dimer (A_1) and trimer (A_2) impurities, suggesting that impurities of small dimensions comparing to the depositing objects, suppress the percolation more successfully comparing to the somewhat longer ones.

In the following, two different methods for determining the critical concentration p_c^* for arbitrary impurity (I) will be described in detail. Let us first focus our attention on the representative results given in table 3 for all examined objects. Table 3 shows the number of independent simulation runs (out of 500) during which the percolation cluster is not formed, for densities $p = 0.1, 0.2, 0.3, 0.4$ of impurity (A_4) and for lattices of size $L = 40-3200$. Note that for the case of low concentrations of impurity $p \leq 0.05$, percolation cluster is formed in each independent simulation run, for all examined objects and lattices. However, the number of simulations that show no percolation rises with increasing the concentration p of impurity (A_4). The absence of percolation is initially visible only in the cases of small lattices. Further increasing of the concentration p leads to the lack of percolation even for the largest lattice, $L = 3200$. In other words, for given object (O) and impurity (I) there is an interval $[p^-(L), p^+(L)]$, where the number of simulations that show no percolation rises from 0% to 100%. Above $p^+(L)$ there is no percolation at all. Conversely, percolation cluster will be formed if the impurity concentration is sufficiently small, i.e. if $p \leq p^-(L)$. It is obvious that these upper and lower bounds of impurity concentrations depend explicitly on the lattice size L . In the following, we shall demonstrate that the interval $[p^-(L), p^+(L)]$ shrinks to a single point

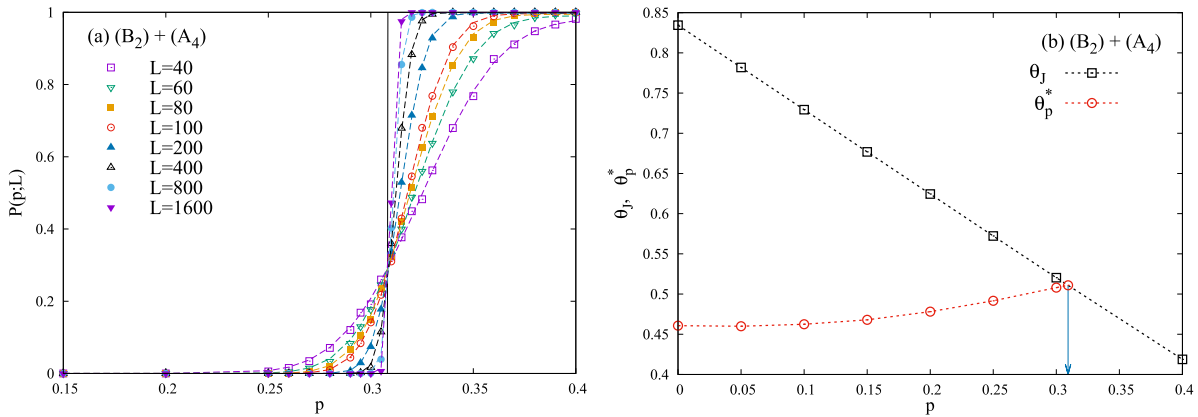


Figure 6. Two methods for determining the critical density p_c : (a) Shown here are the values of the probability $P(p; L)$ that the percolation cluster of deposited objects (B_2) (table 2) is not formed during the simulation run on the lattice of size L (see legend), initially covered with impurities (A_4) (table 1) at various densities p . The dashed superimposed lines are the fits according to equation (2). The thin vertical line indicates the value of fitting parameter $\mu = 0.3081 \pm 0.0008$. (b) Dependences of the jamming density θ_J and the percolation threshold θ_p^* for object (B_2) on the density p of impurity (A_4). The thin vertical arrow indicates the value of critical density $p_c^* = 0.3093$.

p_c^* as the lattice size rises, $L \rightarrow \infty$. Also, it will be shown that this limiting value p_c^* corresponds to the critical concentration of impurities.

Figure 5(a) shows the values of the probability $P(p; L)$ that the percolation cluster of deposited objects (A_2) is not formed during the simulation run on a lattice of size L , initially covered with impurities (A_7) at various concentrations p . The probabilities $P(p; L)$ are determined from $N = 5000$ independent runs for each of the investigated concentrations $p = 0.15-0.40$ of impurity (A_7). Comparing the probabilities $P(p; L)$ for various lattice sizes $L = 40-1600$, one can see that the growth of the probability $P(p; L)$ from 0 to 1 occurs in a narrow density range $[p^-(L), p^+(L)]$ for the larger lattices, i.e. $|p^+(L) - p^-(L)| \rightarrow 0, L \rightarrow \infty$. For other objects and impurities from tables 2 and 1, we get qualitatively the same results for the behavior of probability $P(p; L)$. As an example, the dependence of the probabilities $P(p; L)$ for deposited object (B_2) on concentration p of impurity (A_4) are shown in figure 6(a) for various lattices of size in the range between $L = 40$ and $L = 1600$. It can be seen that the probabilities $P(p; L)$ obtained for object (B_2) and impurity (A_4) (figure 6(a)) are narrower and shifted to higher values of concentration p compared to the probabilities $P(p; L)$ corresponding to object(A_2) + impurity(A_7) case (figure 5(a)).

We have performed a three-parameter fitting of our simulation data for probabilities $P(p; L)$ in order to analyze its behavior for an infinite system $L \rightarrow \infty$. The fitting function we have used is of the form:

$$P(p; L) = \frac{1}{2} \left(1 + \operatorname{erf} \left(\frac{p - \mu}{\sigma\sqrt{2}} - \delta \right) \right), \quad (2)$$

where μ , σ , and δ are the fitting parameters, and $\operatorname{erf}(x)$ is the error function. If $\delta = 0$, the fitting function (2) is identical to the cumulative distribution function (CDF) for the normal (Gaussian) distribution with mean μ and deviation σ :

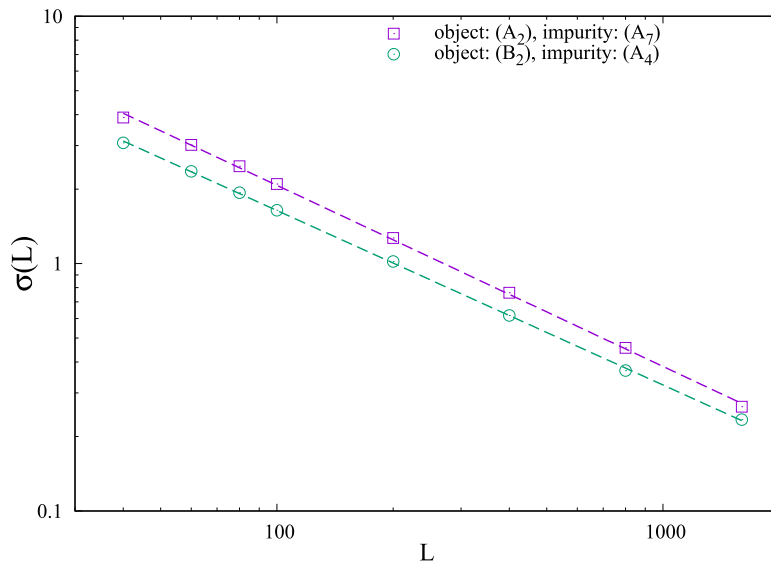


Figure 7. Parameter σ of the fitting function (2), as function of lattice size L , for two pairs $(A_2) + (A_7)$ (squares) and $(B_2) + (A_4)$ (circles), as indicated in the legend. The straight lines are the fits using equation (4). Parameter $\sigma(L)$ seems to be well described by a simple power law. The corresponding values of the exponent γ and the parameter A are: (a) $\gamma = 0.732$ and $A = 60.35$, for $(A_2) + (A_7)$; (b) $\gamma = 0.705$ and $A = 42.21$, for $(B_2) + (A_4)$.

$$P(p; L) = \frac{1}{\sqrt{2\pi}\sigma} \int_{-\infty}^p \exp \left[-\frac{1}{2} \left(\frac{p' - \mu}{\sigma} \right)^2 \right] dp'. \quad (3)$$

This functional form is commonly used to describe the probability P_{perc} to find a percolating cluster on a finite lattice of size L [38–40]. Furthermore, it has been suggested that the probability P_{jam} to find a jamming phase and the fluctuations of the jamming coverage may obey relationship similar to equation (3) [40–42]. Note that the parameter δ in equation (2) determines the probability $P(\mu; L)$ when a critical concentration of impurities μ is reached on a finite lattice of size L . The analysis of the behavior of probabilities $P(p; L)$ is carried out by using the nonlinear fitting routine `FMINSEARCH` in MATLAB[®] (MathWorks, Natick, MA).

Now, it is necessary to establish a connection between the proposed fitting function (2) and the critical concentrations of impurities. The results obtained for all analyzed objects (O) and impurities (I) have shown that the parameter μ does not depend on the size L of the lattice, but depends on the selected pair $(O) + (I)$. The corresponding values of parameter μ for pairs $(A_2) + (A_7)$ and $(B_2) + (A_4)$ are $\mu = 0.2821 \pm 0.0010$ and $\mu = 0.3081 \pm 0.0008$, respectively. These values are denoted by thin vertical lines in figures 5(a) and 6(a). The parameter δ does not depend on the lattice size L and has a value of $\delta \approx 0.3$, for all objects and impurities. However, the parameter σ depends explicitly on the lattice size L . In figure 7 the values of the fitting parameter σ versus the lattice size L are reported for the simulation results shown in figures 5(a) and 6(a). Here, dependence of the parameter σ on the lattice size L is shown on a double logarithmic scale. For all examined objects and impurities these plots are straight lines

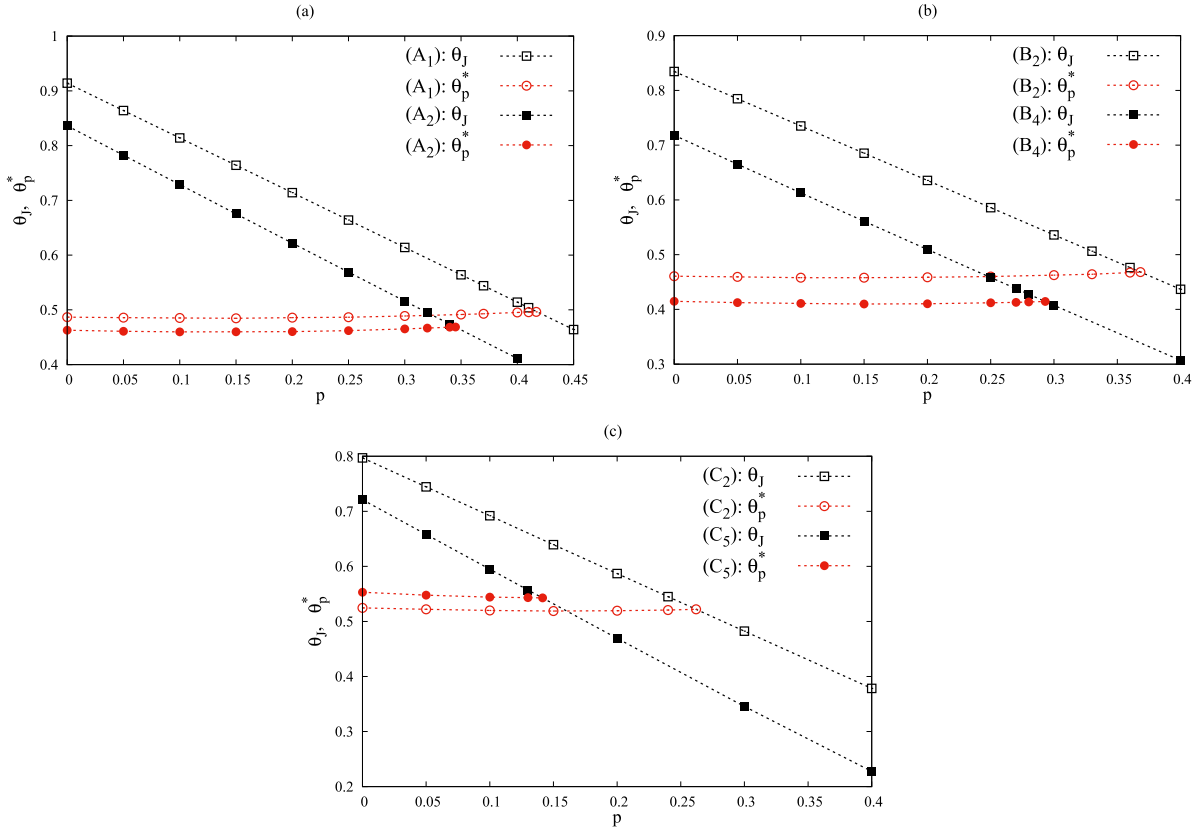


Figure 8. The jamming coverage θ_J and the percolation threshold θ_p^* for objects (a) $(A_1), (A_2)$, (b) $(B_2), (B_4)$, and (c) $(C_2), (C_5)$ from table 2, and impurity (A_1) (table 1).

approximately parallel to each other, indicating that the fitting parameter σ is a simple power-law of the lattice size L :

$$\sigma = A L^{-\gamma}. \tag{4}$$

The corresponding values of the exponent γ for pairs $(A_2) + (A_7)$ and $(B_2) + (A_4)$ are $\gamma = 0.732$ and $\gamma = 0.705$, respectively. For all examined objects and impurities we have obtained the confirmation of the power law of equation (4) with the value of the exponent γ ranging from 0.70 to 0.77. The parameter A depends both on the chosen object (O) and impurity (I).

According to equation (4), in the limit $L \rightarrow \infty$, we have

$$\frac{p - \mu}{\sigma} \rightarrow \begin{cases} -\infty, & p < \mu \ (L \rightarrow \infty) \\ +\infty, & p > \mu \ (L \rightarrow \infty). \end{cases} \tag{5}$$

Since $\text{erf}(-\infty) = -1$ and $\text{erf}(+\infty) = +1$, from equation (2) we obtain that

$$P(p; L \rightarrow \infty) = \begin{cases} 0, & p < \mu \\ 1, & p > \mu. \end{cases} \tag{6}$$

Hence, in the limit $L \rightarrow \infty$ the probability $P(p; L)$ (equation (2)) converges to the discontinuous Heaviside step function (6), indicating that the parameter μ represents the critical impurity concentration p_c^* .

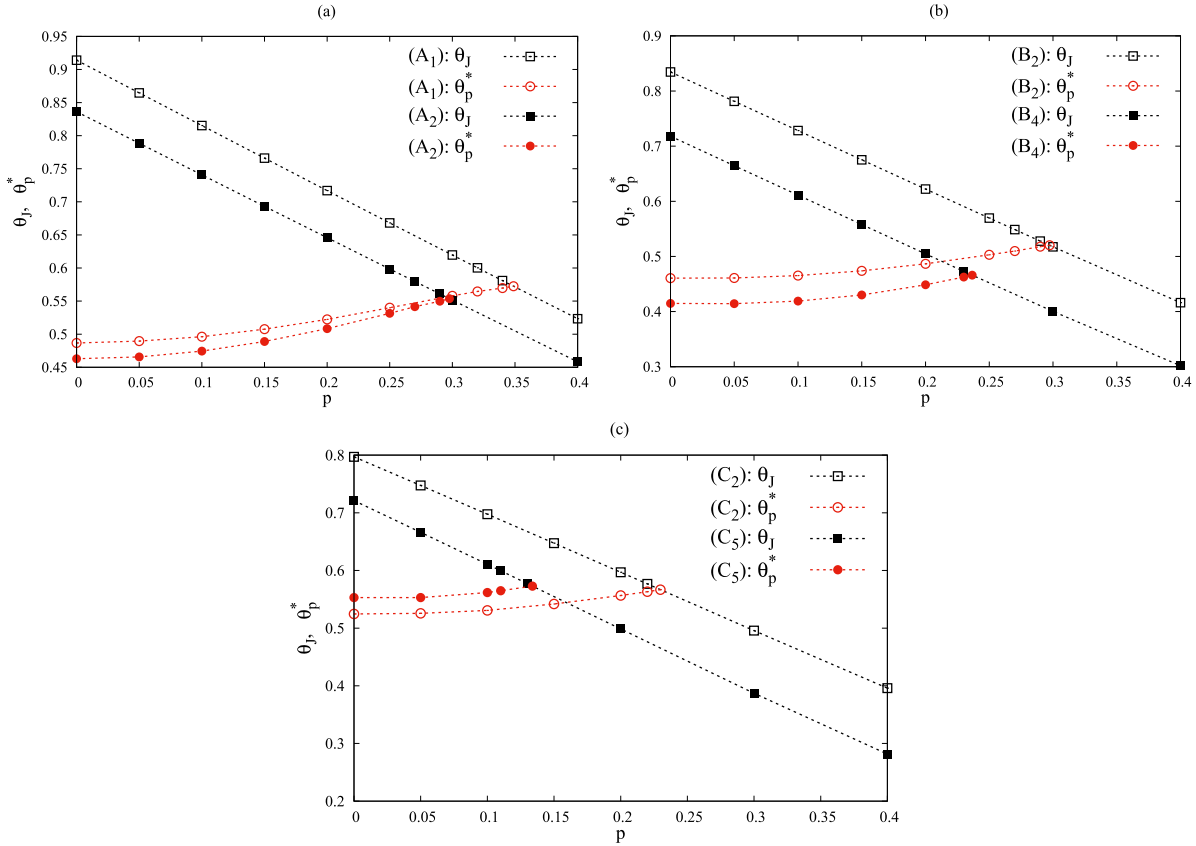


Figure 9. The jamming coverage θ_J and the percolation threshold θ_p^* for objects (a) (A_1) , (A_2) , (b) (B_2) , (B_4) , and (c) (C_2) , (C_5) from table 2, and impurity (A_5) (table 1).

An alternative method for determining the critical concentrations p_c^* is demonstrated in figures 5(b) and 6(b). In these figures, the dependences of jamming density θ_J and percolation threshold θ_p^* on the concentration of impurities p are shown for the following pairs: object (A_2) + impurity (A_7) (figure 5(b)), and object (B_2) + impurity (A_4) (figure 6(b)). As can be seen, for sufficiently large impurity concentrations, the curves $\theta_J(p)$ and $\theta_p^*(p)$ intersect each other at some point. Abscissa of the intersection point $\theta_p^*(p) \cap \theta_J(p)$ is equal to the critical concentration p_c^* of impurity, and its ordinate corresponds to the ‘critical percolation threshold’, denoted by θ_p^c . The critical threshold θ_p^c coincides with the value of the jamming density θ_J when $p = p_c^*$. Our simulations confirm that the percolation threshold θ_p^* can be arbitrarily close to the critical value θ_p^c , if the concentration p of impurities is sufficiently close to the critical value p_c^* . Values of the critical concentration p_c^* obtained in the intersection point $\theta_p^*(p) \cap \theta_J(p)$ for pairs $(A_2) + (A_7)$ and $(B_2) + (A_4)$ are $p_c^* = 0.2815$ and $p_c^* = 0.3093$, respectively. These values are denoted by thin vertical arrows in figures 5(b) and 6(b). It is important to notice that the critical concentrations p_c^* obtained from the analysis of the probability $P(p; L)$ (equation (2)) and determined from the intersection point $\theta_p^*(p) \cap \theta_J(p)$ have practically the same value.

Numerical simulations for all objects and impurities produce qualitatively similar results for the dependence of the jamming density $\theta_J(p)$ and percolation threshold $\theta_p^*(p)$ on the concentration p of impurities. Some examples are given in figures 8 and 9 where

The study of percolation with the presence of extended impurities

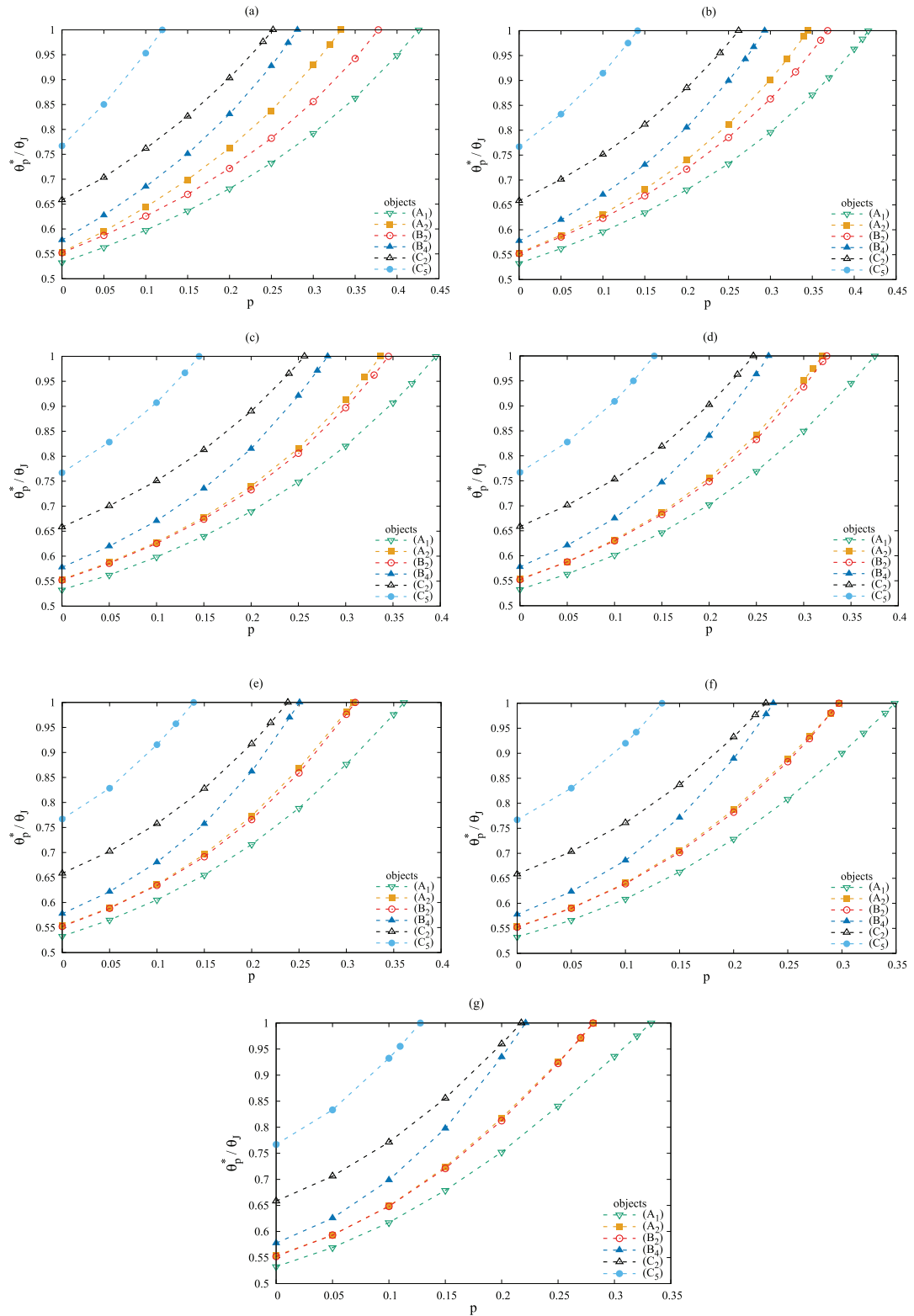


Figure 10. Dependence of the ratio of the percolation threshold and the jamming coverage, θ_p^*/θ_J , on the density p of impurities (a) (A_0) , (b) (A_1) , (c) (A_2) , (d) (A_3) , (e) (A_4) , (f) (A_5) , (g) (A_7) , for all objects in table 2 (see legend).

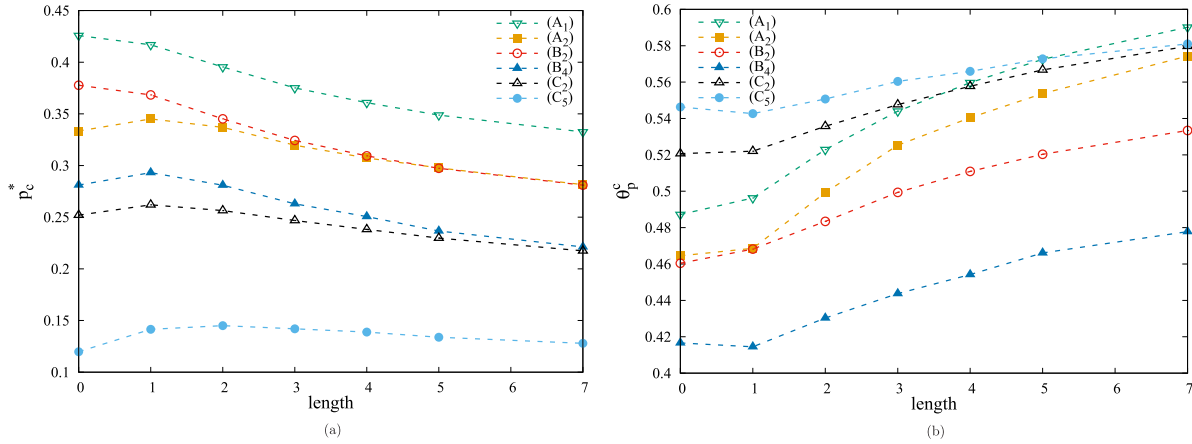


Figure 11. (a) Critical concentrations p_c^* of impurities, and (b) critical percolation thresholds θ_p^c versus the length l of impurities (see table 1) for various objects from table 2.

we have plotted both the jamming density $\theta_J(p)$ and the percolation threshold $\theta_p^*(p)$ for all examined objects (see table 2) as functions of concentration p of the impurities (A_1) and (A_5). As can be seen, from extrapolation of the curve $\theta_p^*(p)$ to the intersection with the curve $\theta_J(p)$, it is always possible to obtain a critical concentration p_c^* for each object and impurity.

We have also considered the ratio of the percolation threshold and the jamming coverage, θ_p^*/θ_J , for all examined pairs of objects and impurities. In figures 10(a)–(g), we show the dependence of the ratio θ_p^*/θ_J on the concentration p of impurities (A_0)–(A_7), for all objects from table 2. As expected, the ratio θ_p^*/θ_J increases with density p for all examined objects, regardless of the length of impurities. The ratio θ_p^*/θ_J increases more sharply for higher impurity concentrations p , and tends to definite value $\theta_p^*/\theta_J = 1$ at the point which corresponds to the critical concentration p_c^* of the impurity.

Figure 11 presents the critical concentrations p_c^* of impurities (figure 11(a)) and the critical percolation thresholds θ_p^c (figure 11(b)) versus the length l of impurities, for various objects from table 2. The critical concentration p_c^* of impurities for reaching percolation generally decreases with the length of impurities because it is more difficult to ‘avoid’ the extended defects. However, in the case of adsorption of larger objects, exception occurs for the point-like impurities (A_0). Indeed, the critical concentration p_c^* of monomers (A_0) is lower than p_c^* for dimer impurities (A_1) in the case of deposition of objects (A_2), (B_4), (C_2), and (C_5). The critical percolation threshold θ_p^c increases with the length l of impurities since a larger coverage of the lattice is needed to form a percolating cluster despite of the presence of impurities. The results for larger objects (B_4) and (C_5) suggest that in the presence of point-like impurities (A_0), critical percolation threshold θ_p^c can have even larger values than in the case of dimer impurities (A_1). The reasons for these results are intuitively clear. The point-like impurities (see figure 1(a)) randomly distributed on the lattice leave enough space for deposition of small objects and forming percolation clusters. Deposition of larger objects is more affected by the presence of these relatively homogeneously distributed impurities. On the other hand, the dimer impurities (see figure 1(b)) are more compact and it is easier to form a

percolating cluster made of large objects at the same effective concentration of impurities. Dimer impurities are also short enough to be easily avoided by the depositing objects. With the growth of impurity length (see figures 1(c) and (d)) it becomes more difficult to avoid them and the critical impurity concentration decreases.

4. Summary

We have investigated percolation phenomena for RSA process with two kinds of deposited particles. One type of particles we considered as finite-size impurities (table 1) that are deposited up to some level in the first stage of the process. Another type of particles were conducting particles that are adsorbed on the substrate contaminated by impurities. These shapes are placed by self-avoiding lattice steps (table 2). We have analyzed how the length ℓ and the concentration p of the needle-like impurity particles changes the percolation threshold θ_p^* of extended conducting particles (k -mers, angled objects and triangles).

For the line segments $((A_1), (A_2))$ and the angled objects $((B_2), (B_4))$ it was shown that the percolation threshold θ_p^* is practically not affected by the presence of point-like impurities (A_0) . However, for sufficiently large impurities, percolation threshold θ_p^* of all examined objects increases with the concentration p . In the case of larger objects, e.g. (C_5) (see figure 4(b)), there is a difference in the behavior of the percolation thresholds θ_p^* for small and large impurities when the concentration of impurities p increases. For small impurities of length $l \leq 3$, percolation threshold θ_p^* of object (C_5) decreases with p for low impurity concentrations; for sufficiently large impurities ($l > 3$) percolation threshold θ_p^* of object (C_5) increases in the whole range of impurity concentrations p . It seems that, at relatively low concentrations p , the presence of small impurities (but not point-like) stimulates the percolation for larger depositing objects.

Special attention has been paid to determining the critical concentration p_c^* of defects above which it is not possible to achieve percolation. It was found that the concentration p_c^* of finite-size impurities for reaching percolation decreases with the length ℓ of impurities. However, exception occurs for larger objects, in which case the critical concentration p_c^* of monomers (A_0) is lower than p_c^* for the dimer impurities (A_1) . We have also shown that the ratio of percolation and jamming thresholds θ_p^*/θ_j increases with impurity concentration p for all examined objects and impurities.

Acknowledgments

This work was supported by the Ministry of Education, Science, and Technological Development of the Republic of Serbia under projects ON171017, III45016, and by the European Commission under H2020 project VI-SEEM, Grant No. 675121. Numerical simulations were run on the PARADOX supercomputing facility at the Scientific Computing Laboratory of the Institute of Physics Belgrade.

References

- [1] Adamczyk Z (ed) 2006 *Particles at Interfaces: Interactions, Deposition, Structure (Interface Science and Technology vol 9)* (Amsterdam: Elsevier)
- [2] Evans J W 1993 Random and cooperative sequential adsorption *Rev. Mod. Phys.* **65** 1281–329
- [3] Privman V 2000 *Colloids Surf. A* **165** 1 (a collection of review articles)
- [4] Talbot J, Tarjus G, Van Tassel P R and Viot P 2000 From car parking to protein adsorption: an overview of sequential adsorption processes *Colloids Surf. A* **165** 287–324
- [5] Cadilhe A, Araújo N A M and Privman V 2007 Random sequential adsorption: from continuum to lattice and pre-patterned substrates *J. Phys.: Condens. Matter* **19** 065124
- [6] Stauffer D and Aharony A 1994 *Introduction to Percolation Theory* (London: Taylor and Francis)
- [7] Grzegorz K and Pekalski A 2001 Percolation and jamming in random sequential adsorption of linear segments on a square lattice *Phys. Rev. E* **63** 051108
- [8] Federica R and Albano E V 2002 Interplay between jamming and percolation upon random sequential adsorption of competing dimers and monomers *Phys. Rev. E* **66** 061106
- [9] Kondrat G 2002 Influence of temperature on percolation in a simple model of flexible chains adsorption *J. Chem. Phys.* **117** 6662
- [10] Kondrat G 2008 Impact of composition of extended objects on percolation on a lattice *Phys. Rev. E* **78** 011101
- [11] Restrepo J G, Ott E and Hunt B R 2008 Weighted percolation on directed networks *Phys. Rev. Lett.* **100** 058701
- [12] Tsakiris N, Maragakis M, Kosmidis K and Argyrakis P 2010 Percolation of randomly distributed growing clusters: finite-size scaling and critical exponents for the square lattice *Phys. Rev. E* **82** 041108
- [13] Cherkasova V A, Tarasevich Y Y, Lebovka N I and Vygornitskii N V 2010 Percolation of aligned dimers on a square lattice *Eur. Phys. J. B* **74** 205–9
- [14] Ziff R M 2009 Explosive growth in biased dynamic percolation on two-dimensional regular lattice networks *Phys. Rev. Lett.* **103** 045701
- [15] Ioselevich A S and Kornyshev A A 2002 Approximate symmetry laws for percolation in complex systems: percolation in polydisperse composites *Phys. Rev. E* **65** 021301
- [16] Araújo N A M and Herrmann H J 2010 Explosive percolation via control of the largest cluster *Phys. Rev. Lett.* **105** 035701
- [17] Tarasevich Y Y, Lebovka N I and Laptev V V 2012 Percolation of linear k -mers on a square lattice: from isotropic through partially ordered to completely aligned states *Phys. Rev. E* **86** 061116
- [18] Budinski-Petković Lj, Lončarević I, Petković M, Jakšić Z M and Vrhovac S B 2012 Percolation in random sequential adsorption of extended objects on a triangular lattice *Phys. Rev. E* **85** 061117
- [19] Cohen R, Erez K, Avraham D B and Havlin S 2001 Breakdown of the internet under intentional attack *Phys. Rev. Lett.* **86** 3682–5
- [20] Newman M E J and Watts D J 1999 Scaling and percolation in the small-world network model *Phys. Rev. E* **60** 7332–42
- [21] Tsukruk V V, Ko H and Peleshanko S 2004 Nanotube surface arrays: weaving, bending, and assembling on patterned silicon *Phys. Rev. Lett.* **92** 065502
- [22] Shim B S and Kotov N A 2005 Single-walled carbon nanotube combing during layer-by-layer assembly: from random adsorption to aligned composites *Langmuir* **21** 9381–5
- [23] Weroński P 2005 Application of the extended RSA models in studies of particle deposition at partially covered surfaces *Adv. Colloid Interface Sci.* **118** 1–24
- [24] Adamczyk Z, Jaszczk K, Michna A, Siwek B, Szyk-Warszyska L and Zembala M 2005 Irreversible adsorption of particles on heterogeneous surfaces *Adv. Colloid Interface Sci.* **118** 25–42
- [25] Cornette V, Ramirez-Pastor A J and Nieto F 2006 Percolation of polyatomic species on site diluted lattices *Phys. Lett. A* **353** 452–8
- [26] Cornette V, Ramirez-Pastor A J and Nieto F 2006 Percolation of polyatomic species with the presence of impurities *J. Chem. Phys.* **125** 204702
- [27] Cornette V, Ramirez-Pastor A J and Nieto F 2011 Random sequential adsorption of polyatomic species with the presence of impurities *Phys. A: Stat. Mech. Appl.* **390** 671–9
- [28] Centres P M and Ramirez-Pastor A J 2015 Percolation and jamming in random sequential adsorption of linear k -mers on square lattices with the presence of impurities *J. Stat. Mech.* **P10011**
- [29] Tarasevich Y Y, Laptev V V, Vygornitskii N V and Lebovka N I 2015 Impact of defects on percolation in random sequential adsorption of linear k -mers on square lattices *Phys. Rev. E* **91** 012109

- [30] Tarasevich Y Y, Laptev V V, Goltseva V A and Lebovka N I 2017 Influence of defects on the effective electrical conductivity of a monolayer produced by random sequential adsorption of linear k -mers onto a square lattice *Phys. A: Stat. Mech. Appl.* **477** 195–203
- [31] Kondrat G 2005 The study of percolation with the presence of impurities *J. Chem. Phys.* **122** 184718
- [32] Kondrat G 2006 The effect of impurities on jamming in random sequential adsorption of elongated objects *J. Chem. Phys.* **124** 054713
- [33] Budinski-Petković Lj, Lončarević I, Jakšić Z M and Vrhovac S B 2016 Jamming and percolation in random sequential adsorption of extended objects on a triangular lattice with quenched impurities *J. Stat. Mech.* **053101**
- [34] Ayala P, Arenal R, Loiseau A, Rubio A and Pichler T 2010 The physical and chemical properties of hetero-nanotubes *Rev. Mod. Phys.* **82** 1843–85
- [35] Wepasnick K A, Smith B A, Bitter J L and Howard F D 2010 Chemical and structural characterization of carbon nanotube surfaces *Anal. Bioanal. Chem.* **396** 1003–14
- [36] Newman M E J and Ziff R M 2000 Efficient Monte Carlo algorithm and high-precision results for percolation *Phys. Rev. Lett.* **85** 4104–7
- [37] Newman M E J and Ziff R M 2001 Fast Monte Carlo algorithm for site or bond percolation *Phys. Rev. E* **64** 016706
- [38] Ramirez L S, Centres P M and Ramirez-Pastor A J 2015 Inverse percolation by removing straight rigid rods from square lattices *J. Stat. Mech.* **P09003**
- [39] Ramirez L S, De la Cruz Flix N, Centres P M and Ramirez-Pastor A J 2017 Dimer site-bond percolation on a triangular lattice *J. Stat. Mech.* **023206**
- [40] Vandewalle N, Galam S and Kramer M 2000 A new universality for random sequential deposition of needles *Eur. Phys. J. B* **14** 407–10
- [41] Loscar E S, Borzi R A and Albano E V 2003 Scaling behavior of jamming fluctuations upon random sequential adsorption *Eur. Phys. J. B: Condens. Matter Complex Syst.* **36** 157–60
- [42] Loscar E S, Borzi R A and Albano E V 2003 Fluctuations of jamming coverage upon random sequential adsorption on homogeneous and heterogeneous media *Phys. Rev. E* **68** 041106